OXFORD CENTRE FOR COLLABORATIVE APPLIED MATHEMATICS

Report Number 11/54

A multiple scales approach to evaporation induced Marangoni convection

by

Matthew G. Hennessey and Andreas Münch

Oxford Centre for Collaborative Applied Mathematics
Mathematical Institute
24 - 29 St Giles'
Oxford
OX1 3LB
England

A MULTIPLE SCALES APPROACH TO EVAPORATION INDUCED MARANGONI CONVECTION*

MATTHEW G. HENNESSY AND ANDREAS MÜNCH†

Abstract. This paper considers the stability of thin liquid layers of binary mixtures of a volatile (solvent) species and a non-volatile (polymer) species. Evaporation leads to a depletion of the solvent near the liquid surface. If surface tension increases for lower solvent concentrations, sufficiently strong compositional gradients can lead to Bénard-Marangoni-type convection that is similar to the kind which is observed in films that are heated from below. The onset of the instability is investigated by a linear stability analysis. Due to evaporation, the base state is time dependent, thus leading to a non-autonomous linearised system, which impedes the use of normal modes. However, the time scale for the solvent loss due to evaporation is typically long compared to the diffusive time scale, so a systematic multiple scales expansion can be sought for a finite dimensional approximation of the linearised problem. This is determined to leading and to next order. The corrections indicate that sufficient separation of the top eigenvalue from the remaining spectrum is required for the validity of the expansions, but not the magnitude of the eigenvalues themselves. The approximations are applied to analyse experiments by Bassou and Rharbi with polystyrene/toluene mixtures [Langmuir 2009 (25) 624–632].

1. Introduction. Convective instabilities play an important role in a number of practical applications and have therefore been the focus of both experimental and theoretical research for many years. The earliest quantitative experiments were undertaken by Bénard [2, 3, 4]. His work inspired Rayleigh [35] to formulate a theory for convective instabilities driven by buoyancy, i.e. by density variations in the liquid that are induced by a thermal gradient. However, experiments by Block [6] and an analytical investigation by Pearson [34] for a one-layer model of a film with a passive gas layer on top and a non-deformable gas/liquid interface showed that the liquid layers in Bénard's experiments were too thin to give rise to buoyancy driven convection, but that an instability can arise from surface tension variations. These initial investigations have spawned continuing scientific interest in convective instabilities; for an overview of the thriving field, see the review by Bodenschatz et al. [7] and the monographs by Colinet et al. [12] and Nepomnyaschy et al. [33].

Pearson's analysis assumes a flat interface and the instability sets in for Marangoni numbers above a critical value. The case of a deformable interface is considered by Scriven and Sternling [38] for a two-layer model; they find it is unstable at all Marangoni numbers with respect to very long waves. Smith [40] shows for a one-layer model that inclusion of gravity suppresses the long-wave instability below a non-zero Marangoni-number. In fact, Pearson's model is regained in the limit of small capillary and large Galileo number, see Davis [14] or Colinet et al. [12]. In this paper, we will focus on models with non-deformable interfaces.

For an evaporating liquid layer, Marangoni-driven convective instabilities can occur even in the absence of external heating if either the latent heat of evaporation induces a temperature gradient that drives the instability, or if the liquid is a mixture with constituents of different volatility and a surface tension that increases as the more volatile species is depleted. In the latter case, the preferred evaporation of one component leads to a concentration gradient which plays a similar role as the temper-

*This publication is based on work supported by Award No. KUK-C1-013-04, made by King Abdullah University of Science and Technology (KAUST). The authors would also like to thank Chris Breward, Colin Please and Barbara Wagner for many helpful discussions.

†Mathematical Institute, University of Oxford, 24-29 St. Giles', Oxford OX1 3LB, UK (muench@maths.ox.ac.uk)

ature gradient. The relevance of compositional Marangoni effects is already discussed by Pearson, but theoretical investigations are less frequent than for the thermocapillary instability, despite the practical importance of the phenomenon for example for the preparation of thin polymer films from dilute solutions [8, 18]; we note in passing that solutal Marangoni effects are also thought to play a role in the levelling of drying paint, see Howison et al. [20]. For a system with two layers of solvent/polymer mixtures (with the same solvent but different immiscible polymers in each of the layers), a linear stability analysis is carried out by Souche and Clarke [42]. Recently, Machrafi et al. [29, 28] have performed a linear stability analysis for a two-layer model for evaporating water/ethanol mixtures with a flat interface; their approach takes into account the instabilities arising from solutal and thermal Marangoni effects as well as from buoyancy.

An aspect that comes into play for evaporating layers is that the concentration profiles and the layer thickness evolve in time as the volatile component is removed. For the linear stability analysis, this means that the base state which is then perturbed is time dependent; as a result, the resulting linearised equations have time dependent coefficients. For such problems, the usual normal modes approach or generalisations where the spatial and temporal variables can be separated only works in exceptional cases such as in the problem studied by Smolka et al. [41] on the extensional motion of a liquid sheet. Floquet theory [5, 36] is designed for time-periodic base flows which is not the case here. One possibility to handle this difficulty is to circumvent it by modifying the model. This approach was chosen by Souche and Clarke [42] who impose a flux at the lower boundary layer that exactly matches the evaporation at the interface. Thus, the model permits stationary base states but the modification remains somewhat ad hoc and its impact on the result needs to be assessed.

A general approach is to solve the linearised system numerically as an initial value problem, used by Foster [17] for buoyancy driven thermal instabilities. For Rayleigh-Marangoni-Bénard convection driven by evaporation, an extension of the amplification method was used by Doumenc et al. [15] and Touazi et al. [43] for a model that includes the temperature gradients induced by the evaporation but not the compositional variations. The results are compared to experiments with polymer solutions by Toussaint et al. [44]. Instead of solving the linearised system for an arbitrary choice of initial perturbation, the optimal choice is determined which maximises the amplification of the energy of the perturbation at a given time. The general method was introduced and explored earlier by a number of authors in particular for problems with steady base states but non-normal linearised operators, where transient amplifications can be larger than the asymptotic behaviour indicated by the linear operator's spectrum, see Schmid and Henningson [37] and references therein. Trouette et al. [45] extend the numerical work to treat the nonlinear model and include other geometries and also stochastic perturbations. Stochastic forcing was treated earlier for convection instabilities in rapidly heated layers by Jhaveri et al. [21].

The question naturally arises if the linearised problem can be treated by some analytical approximation. An analytic approach to the initial phase where the base state changes rapidly but where the gradient is confined to a thin boundary layer was carried out by Kang et al. [22] for a case of Bénard-Marangoni convection for a horizontal liquid layer that is suddenly cooled from above. They use a propagation method that essentially seeks the solution of the linearised problem in the evolving boundary layer.

On the other hand, after the boundary layer has penetrated the film, the base

state often settles into a quasi-equilibrium, where further changes of the gradient are slow compared to the time scale of the instability. For the concentration field, this happens specifically if the solvent loss due to evaporation occurs on a much longer time than diffusion. This has been exploited for example by the "frozen" time approach. The time dependence of the coefficients in the linearised equation is neglected but retained for the perturbation itself. This system can be solved by normal modes and the solution will grow or decay depending on the sign of the real part of the leading eigenvalue. This approach has been used by Lick [26] and Currie [13] to investigate thermal convective instabilities (and also by Kang et al. [22] for late times), and by Machrafi et al. [29, 28] in their work on evaporating water/ethanol mixtures.

In this approach, the eigenvalues are effectively treated as constant while, in fact, they slowly change as the base state evolves. This implies that it is possible for modes which are initially unstable to stabilise in the long term. It has been repeatedly observed that by integrating the eigenvalue in time and using this as the argument of the exponential function rather than its initial value multiplied by time, an often surprisingly good approximation of the evolution of the perturbation can be obtained. In particular, this approximation is able to capture the change from growth to decay or vice-versa if the leading eigenvalue changes sign. This or similar approximations have been used for example by Lick [26], Mahler et al. [30], Warner et al. [47] and Edmonstone et al. [16], and King et al. [25] and Münch et al. [31] for a range of different problems where the base state changes slowly. It is tempting to think that this approximation can be justified by one of the techniques using expansions with multiple time scales as in Kevorkian [23], or Kevorkian and Cole [24]. However, as far as we know, this has not been done for the type of slowly changing base states as they arise in convective instabilities, though we note that multiple scale ideas have been used in the context of boundary layer instabilities where the boundary layer varies slowly in space, for example by Bouthier [10, 11]. In our paper, we will show how the intuitive result can be recovered from a systematic multiple scale approach including higher order corrections that provide insight into the validity of the approximation.

Other approaches that account for the slow change of the base state include for example Shen's work [39], who investigates the stability of an incompressible time-dependent flow (inviscid and viscous) by considering the ratio of the kinetic energy of the perturbation velocity field to the energy of the (time-dependent) velocity profile. The derivative of the log of this quantity is then a measure of growth or decay of the perturbation relative to the base state that can be expressed as the sum of the leading "frozen time" eigenvalue and a contribution from the evolving base state. Stability boundaries using energy stability concepts without requiring a separation of time scales were also derived by Homsy et al. [19] for convective instabilities.

The layout of the paper is as follows. In section 2, we formulate a model for an evaporating (laterally infinite) liquid layer consisting of a solution of a non-volatile polymer in a volatile solvent, with a passive gas on top. We restrict ourselves to the simplest model with a flat, non-deformable interface and where the surface tension is assumed to depend only on the composition. We thus neglect thermal Marangoni as well as buoyancy effects. Evaporation is assumed to be small on the diffusive time scale, leading to a small Biot number on which the subsequent asymptotic analysis is built. In section 3, we determine asymptotic approximations of the base state to leading order in the Biot number and compare them with numerical results. In section 4, we linearise the model about the full time dependent base state and then reduce the initial value problem to a finite dimensional ODE system by projecting it

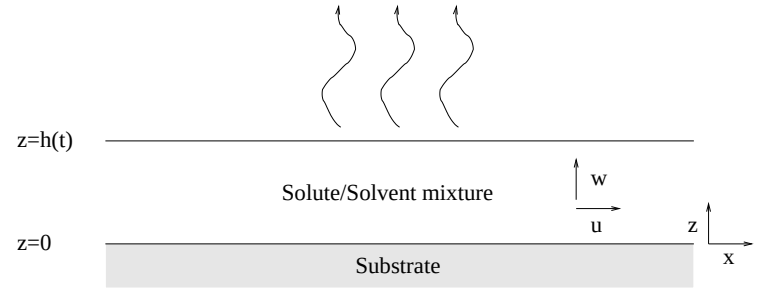

FIG. 2.1. *Sketch of the physical situation with a thin liquid layer consisting of a mixture of a volatile solvent and a non-volatile polymer.*

onto the leading modes of the slowly evolving eigenvalue problem. We then exploit the separation of time scales to obtain asymptotic approximations for this system and thus for the full linearised initial value problem via multiple scale expansions. We also solve the linearised system numerically and compare the solutions with the asymptotic approximations. In section 5, we use our results to discuss the experiments by Bassou and Rharbi [1]. We finally conclude in section 6.

2. Mathematical Model.

Governing equations. We consider a liquid film consisting of a mixture of a volatile solvent and a non-volatile polymer. Coordinates x and z are introduced as shown in the fig. 2.1, and t represents time. Bulk equations for the pressure field $p = p(x, z, t)$, the two components of the velocity $u = u(x, z, t)$ and $w = w(x, z, t)$ (as shown in the sketch), and the concentration of the solvent $c = c(x, z, t)$ consist of the Stokes equations, an incompressibility condition that corresponds to conservation of mass, and a convection/diffusion equation for the concentration field:

$$-\nabla p + \mu \Delta \boldsymbol{u} = 0, \tag{2.1}$$

$$\nabla \cdot \boldsymbol{u} = 0, \tag{2.2}$$

$$c_t + \boldsymbol{u} \cdot \nabla c = D \Delta c, \tag{2.3}$$

where $\boldsymbol{x} = (x, z)$ and $\boldsymbol{u} = (u, w)$, $\nabla = (\partial_x, \partial_z)$ and $\Delta = \nabla^2 = \partial_x^2 + \partial_z^2$. Also, μ is the dynamic viscosity of the liquid and D the diffusion coefficient for the solvent, both of which we assume to be independent of the concentration.

At $z = 0$, i.e. at the surface of the substrate, we assume no-slip for the horizontal velocity component and for the other component that the substrate is impermeable for both constituents of the liquid, so that

$$\boldsymbol{u} = 0, \qquad c_z = 0. \tag{2.4}$$

We will assume that the interface is non-deformable and thus given as $z = h(t)$. Non-deformability has been frequently used in studies of thermally driven Bénard-Marangoni convection under conditions where surface tension and gravity are strong enough to keep the interface flat [14].

At $z = h(t)$, we impose the kinematic condition and we assume that the only volatile component is the solvent, which evaporates from the liquid at a rate that is proportional to its concentration. This simple relation for the evaporation rate is phenomenological and motivated by applications in spin-coating [9]. It was also

used by Souche and Clarke in their investigation of Marangoni instabilities for a two-layer film of liquid mixtures with an evaporating solvent [42]. Thus, the boundary conditions are

$$\begin{aligned} \rho(\boldsymbol{u}\cdot\boldsymbol{e_z} - h_t) &= k_m c \\ c(\boldsymbol{u}\cdot\boldsymbol{e_z} - h_t) - D\nabla c\cdot\boldsymbol{e}_z &= k_m c. \end{aligned} \tag{2.5}$$

The symbols $\boldsymbol{e_x}$ and $\boldsymbol{e_z}$ denote the unit vectors in the direction of the x and z axis, respectively. We neglect variations of the density between the two species so that the density of the mixture ρ is kept constant. We replace the last equation by its sum with (2.5), which has a slightly more compact form

$$D\nabla c\cdot\boldsymbol{e}_z = -k_m(1-c/\rho)c. \tag{2.6}$$

The concentration gradients along the liquid/air interface induces a Marangoni shear stress,

$$\mu\,\boldsymbol{e_x}\cdot(\nabla\boldsymbol{u} + \nabla\boldsymbol{u}^T)\cdot\boldsymbol{e_z} = -\gamma_c\nabla c\cdot\boldsymbol{e}_x. \tag{2.7}$$

Here, we have assumed that surface tension decreases linearly with increasing concentration of the solvent, so that γ_c is a positive parameter.

Finally, we have initial conditions at $t = 0$,

$$h(0) = h_i, \qquad c(x,z,0) = c_i(x,z), \tag{2.8}$$

with some specified thickness h_i and initial concentration field c_i. We denote the mean value of the initial concentration field by

$$c_m = \lim_{L\to\infty}\frac{1}{2h_iL}\int_{-L}^{L}\int_0^{h_i} c_i(x,z)dzdx. \tag{2.9}$$

Non-dimensionalisation. We non-dimensionalise the governing equations using the initial film thickness h_i as the length scale for x, z and h, the diffusive time scale h_i^2/D for t, the ratio of the two, D/h_i, as the velocity scale for u and w and the pressure scale $\mu D/{h_i}^2$ for p. For the concentration field, we write $c = c_m + h_i c_s\tilde{c}$, where c_s measures the typical concentration gradient. Notice that for a well mixed fluid $\tilde{c}_i = 0$. An estimate for the concentration gradient can be obtained from (2.6), if we replace c by its initial mean value c_m, yielding $|c_z| \sim k_m(1-c_m/\rho)c_m/D \equiv c_s$. With these scalings, we obtain the equations for the bulk (after dropping the tildes from c and c_i),

$$-p_x + u_{xx} + u_{zz} = 0, \tag{2.10a}$$
$$-p_z + w_{xx} + w_{zz} = 0, \tag{2.10b}$$
$$u_x + w_z = 0, \tag{2.10c}$$
$$c_t + uc_x + wc_z = c_{xx} + c_{zz},. \tag{2.10d}$$

For the boundary conditions at $z = 0$ we find

$$u = 0, \qquad w = 0, \qquad c_z = 0, \tag{2.10e}$$

and at the liquid gas interface $z = h(t)$,

$$w - h_t = \delta\beta(1+\delta(1-\beta)c), \tag{2.10f}$$
$$c_z = -(1+\delta(1-\beta)c)(1-\delta\beta c), \tag{2.10g}$$
$$u_z + w_x = -\mathrm{Ma}\,c_x; \tag{2.10h}$$

the initial conditions are

$$h(0) = 1, \qquad c(x, z, 0) = c_i(x, z), \tag{2.10i}$$

where the latter is now assumed to have a mean value zero. Three parameters appear in this system,

$$\beta = c_m/\rho, \qquad \delta = \frac{k_m h_i}{D}, \qquad \mathrm{Ma} = \delta \frac{\beta(1-\beta)\gamma_c \rho h_i}{\mu D}. \tag{2.11}$$

These are the initial solvent volume fraction, the evaporative Biot number, and the Marangoni number, respectively. In this paper, we will consider the limit of small Biot-number, $0 < \delta \ll 1$, while keeping β and Ma fixed.

3. Base state. We seek one-dimensional solutions of (2.10a)-(2.10i), i.e. solutions for which u is zero and w, c, p do not depend on x. We find that $w = 0$, $p = 0$, while $c = C(z, t)$ satisfies a diffusion equation in the bulk,

$$C_t = C_{zz} \tag{3.1a}$$

and the boundary and initial conditions

$$C_z(0, t) = 0, \tag{3.1b}$$
$$h_t(t) = -\delta\beta(1 + \delta(1-\beta)C(h(t), t)), \tag{3.1c}$$
$$C_z(h(t), t) = -(1 + \delta(1-\beta)C(h(t), t))(1 - \delta\beta C(h(t), t)), \tag{3.1d}$$
$$h(0) = 1, \qquad C(z, 0) = 0. \tag{3.1e}$$

In the following, we seek asymptotic solutions to this system of equations for small Biot numbers $\delta \ll 1$ and fixed initial volume fraction β, and compare them to numerical solutions. It turns out that we need to consider two time regimes. In the first, the concentration field forms a boundary layer that quickly penetrates the film and then reaches a quasi-equilibrium, while the film thickness remains constant to leading order. In the second, i.e. the slow time regime, the leading order solution for the thickness and the leading contribution to concentration gradient decrease as a result of the loss of solvent due to evaporation.

3.1. Early time regime $t = O(1)$. Brief inspection of the equations show that the solution is trivial unless we balance the left and right hand side of (3.1d). We therefore expand C and h as

$$C(z, t) = C_0(z, t) + \delta C_1(z, t) + \cdots, \qquad h(t) = h_0(t) + \delta h_1(t) + \cdots. \tag{3.2}$$

The leading order problem is

$$C_{0,t} = C_{0,zz} \tag{3.3a}$$
$$C_{0,z}(0, t) = 0, \tag{3.3b}$$
$$h_{0,t}(t) = 0, \tag{3.3c}$$
$$C_{0,z}(h_0(t), t) = -1, \tag{3.3d}$$
$$h_0(0) = 1, \qquad C_0(z, 0) = 0. \tag{3.3e}$$

This shows that in this time regime, h_0 is constant and equal to one, while C_0 satisfies the heat equation thus can be found by series expansions. Moreover, we can easily see that

$$\int_0^1 C_0(z, t) dz = -t. \tag{3.4}$$

Using this mass-balance relation and (3.3a), (3.3b), one finds that the long-time asymptotic behaviour $t \to \infty$ for the leading order solution is

$$h_0(t) \sim 1, \qquad C_0(z,t) \sim -z^2/2 + 1/6 - t, \tag{3.5}$$

in order to match into the next time regime.

3.2. Late time regime $t = O(\delta^{-1})$. The previous regime breaks down at $t = O(\delta^{-1})$ when evaporation begins to have a significant effect on the film thickness h_0. We rescale $t = \tau/\delta$ and expand

$$C(z,\tau) = \delta^{-1} C_0(z,\tau) + C_1(z,\tau) + \cdots, \qquad h(\tau) = h_0(\tau) + \delta h_1(\tau) + \cdots. \tag{3.6}$$

The leading order problem is

$$C_{0,zz} = 0, \tag{3.7a}$$
$$C_{0,z}(0,\tau) = 0, \tag{3.7b}$$
$$h_{0,\tau}(\tau) = -\beta\left[1 + (1-\beta) C_0(h_0(\tau),\tau)\right], \tag{3.7c}$$
$$C_{0,z}(h_0(\tau),\tau) = 0, \tag{3.7d}$$
$$h_0 \sim 1, \qquad C_0 \sim -\tau \qquad \text{for } \tau \to 0; \tag{3.7e}$$

the last equation comes from matching to the initial time layer. The solution of (3.7) is

$$C_0(z,\tau) = C_0(\tau), \qquad h_0(\tau) = 1 - \beta\tau - \beta(1-\beta)\int_0^\tau C_0(s)ds, \tag{3.8}$$

with a C_0 that is independent of z. The precise functional form for C_0 needs to be determined from a solvability condition arising from the next order problem, the relevant parts of which are

$$C_{1,zz} = C_{0,\tau}, \tag{3.9a}$$
$$C_{1,z}(0,\tau) = 0, \tag{3.9b}$$
$$C_{1,z}(h_0(\tau),\tau) = -\left[1 + (1-\beta)C_0(\tau)\right]\left[1 - \beta C_0(\tau)\right]. \tag{3.9c}$$

Integrating (3.9a) and using (3.7c) to express the resulting right hand side in terms for $h_{0,\tau}$ yields $(h_0 C_0)_\tau = h_{0,\tau}/\beta$, and therefore

$$C_0 = -\frac{(1-h_0)}{\beta h_0}. \tag{3.10}$$

Using this in (3.7c) and gives an ODE for h_0 which has the implicit solution

$$h_0 - 1 + (1-\beta)\ln\left[\frac{h_0 - (1-\beta)}{\beta}\right] = -\tau. \tag{3.11}$$

The system (3.9) has the solution

$$C_1(z,\tau) = -\frac{h_0 - 1 + \beta}{2\beta h_0^3}\, z^2 + C_1(0,\tau), \tag{3.12}$$

stated here in terms of h_0. The function $C_1(0,\tau)$ is fixed by a solvability condition for the second order problem. We do not determine it here since it will not be required for the linear stability analysis in section 4.

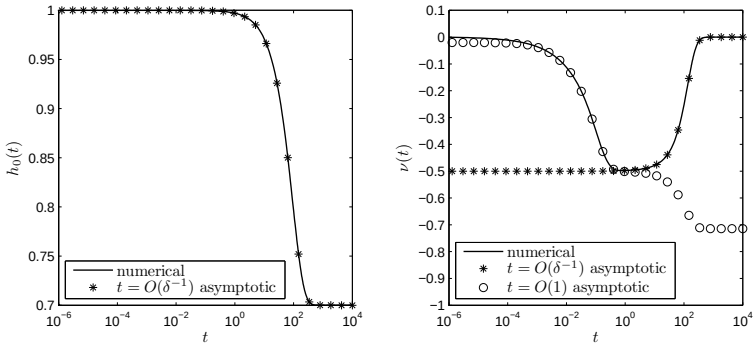

FIG. 3.1. *Comparison of the asymptotic approximations (correct to $O(\delta)$) with numerical solutions of the base state for the full one dimensional equations* (3.1). *The film thickness is shown in the left and the average concentration gradient (explained in the text) in the right figure. Note that the leading order for h_0 for $t = O(1)$ is trivial and has therefore been omitted on the left.*

We now compare these asymptotic results with numerical results for (3.1) for $\delta = 0.01$ and $\beta = 0.3$. This initial volume fraction of solvent is somewhat small, most physical experiments use solutions where the initial content of polymer is typically on the order of a few percent. The important features of the evolution do not critically depend on the value of β so we will keep $\beta = 0.3$ for most of this paper. However, in section 5, where we compare with experiments by Bassou and Rharbi [1], we will use a β that is much closer to one.

Here, we specifically look at the evolution of the film thickness $h(t)$ and the average concentration gradient $\nu(t) = (c(h(t), t) - c(0, t))/h(t)$. We clearly see that for t less or equal than about one, the film thickness remains approximately constant while the concentration gradient builds up until it plateaus at slightly less than $t = 1$. This in good qualitative and quantitative agreement with the asymptotic solution for the $t = O(1)$ time regime. At later times, in fact shortly after $t = 1$, the evolution is captured by the asymptotic results of the $t = O(\delta^{-1})$ regime where the film thickness and the concentration change slowly until the solvent reaches depletion at a very late stage.

Therefore, the concentration gradient can be assumed to vary only slowly in time for $t \gg 1$. We will exploit this to obtain approximations to the solutions of the linearised equations for small perturbations of the one-dimensional base state in the next section.

4. Linear stability.

4.1. Formulation. We will now investigate the stability of the base state by examining how two-dimensional perturbations to this state evolve in time. It will be assumed that these perturbations remain sufficiently small that the equations can be linearised about the basic state.

In particular, we seek a solution to the governing equations of the form

$$u(x,z,t) = \alpha \int_{-\infty}^{\infty} \hat{u}(z,t;k) e^{ikx} dk, \tag{4.1a}$$

$$w(x,z,t) = \alpha \int_{-\infty}^{\infty} \hat{w}(z,t;k) e^{ikx} dk, \tag{4.1b}$$

$$p(x,z,t) = \alpha \int_{-\infty}^{\infty} \hat{p}(z,t;k) e^{ikx} dk, \tag{4.1c}$$

$$c(x,z,t) = C(z,t) + \alpha \int_{-\infty}^{\infty} \hat{c}(z,t;k) e^{ikx} dk, \tag{4.1d}$$

$$h(t) = h(t) + \alpha \int_{-\infty}^{\infty} \hat{h}(t;k) e^{ikx} dk, \tag{4.1e}$$

where $0 < \alpha \ll 1$. Since we have assumed that the liquid/air interface remains flat, $\hat{h}(t;k)$ is proportional to a delta function. We are interested in perturbations that can give rise to laterally non-trivial patterns, and therefore restrict our attention to the case $k \neq 0$, where $\hat{h}(t;k)$ is zero.

We insert this ansatz into (2.10) and expand. To $O(1)$, we recover the equations for the base state (3.1). After eliminating $\hat{u}$, the $O(\alpha)$ equations in the bulk are

$$\hat{p}_{zz} - k^2 \hat{p} = 0, \tag{4.2a}$$

$$\hat{w}_{zz} - k^2 \hat{w} = \hat{p}_z, \tag{4.2b}$$

$$\hat{c}_t + \hat{w} C_z = \hat{c}_{zz} - k^2 \hat{c}, \tag{4.2c}$$

with boundary conditions at $z = 0$,

$$\hat{w} = 0, \quad w_z = 0, \quad \hat{c}_z = 0, \tag{4.2d}$$

and at $z = h(t)$,

$$\hat{w} = \delta^2 \beta (1-\beta) \hat{c}, \tag{4.2e}$$

$$\hat{c}_z = -\delta \left[1 - 2\beta - 2\delta\beta(1-\beta) C \right] \hat{c}, \tag{4.2f}$$

$$\hat{p}_z = -k^2 (\mathrm{Ma} + 2\delta^2 \beta (1-\beta)) \hat{c}. \tag{4.2g}$$

The initial condition is

$$\hat{c}(z,0;k) = \hat{c}_i(z;k). \tag{4.2h}$$

Also notice that we can solve (4.2a), (4.2b), (4.2d), (4.2e) and (4.2f) for $\hat{w}$ and $\hat{p}$ and that the solution for the former can be written as $\hat{c}(h(t),t)$ times a function of z and of time, say $g(z,\tau;\mathrm{Ma},\delta)$, that is independent of $\hat{c}$. The time dependence of this function enters due to the evolving domain i.e. via boundary conditions imposed at $z = h$. We do not give the explicit expression for g here, since it is not particularly interesting. With the help of g, we can reduce the linearised problem to one for $\hat{c}$ only,

$$\hat{c}_t(z,t) = \hat{c}_{zz}(z,t) - k^2 \hat{c}(z,t) - \hat{c}(h(\tau),t) g(z,\tau;\mathrm{Ma},\delta) C_z(z,\tau), \tag{4.3a}$$

$$\hat{c}_z(0,t) = 0, \tag{4.3b}$$

$$\hat{c}_z(h(\tau),t) = -\delta \left[1 - 2\beta - 2\delta\beta(1-\beta) C(\tau,\delta) \right] \hat{c}(h(\tau),t), \tag{4.3c}$$

$$\hat{c}(z,0) = \hat{c}_i(z). \tag{4.3d}$$

For future reference, we introduce a bulk and a boundary operator, $\mathcal{L}(\tau,\delta)$ and $\mathcal{B}(\tau,\delta)$, respectively, so that (4.3a) can be written as $\hat{c}_t(z,t) = \mathcal{L}(\tau,\delta)\,\hat{c}(z,t)$ and the boundary conditions (4.3b), (4.3c) as $\mathcal{B}(\tau,\delta)\hat{c}(z,t) = 0$.

4.2. Reduction to a finite dimensional system. For each wavenumber k, the system (4.3) represents an initial/boundary value that is coupled to the initial/boundary value problem for the base state (3.1) and that needs be solved for any initial perturbation $\hat{c}_i(z)$ and wavenumber k. If the perturbation undergoes sufficient amplification, the base state would be deemed to be unstable with respect to this perturbation. Such a solution can be obtained numerically, but we also seek asymptotic approximations that exploit the slow evolution of the base state in the time regime $t = O(\delta^{-1})$. For this reason, we have expressed the base state variables C and h in (4.3) in terms of the slow time $\tau = \delta t$.

We now approximate $\hat{c}$ by first expanding in terms of the eigenfunctions of $(\mathcal{L},\mathcal{B})$ using only the first N leading modes (i.e. the eigenfunctions for the eigenvalues with the largest real part),

$$\hat{c}(z,t) \approx \sum_{j=1}^{N} c_j(t) v_j(z;\tau). \tag{4.4}$$

If the spectrum of the operator is discrete and the eigenfunctions form a complete set, we can expect this representation of $\hat{c}$ to become exact if $N \to \infty$. If the modes included in (4.4) are sufficiently well separated from the neglected part of the spectrum, we will usually only need a few modes to obtain a good approximation of $\hat{c}$ for all but perhaps very early times.

The eigenvalues $\lambda = \lambda_j$ and the eigenfunctions $v = v_j$ satisfy

$$\mathcal{L}(\tau,\delta)\,\hat{v} = \lambda v, \tag{4.5a}$$
$$\hat{v}_z = 0 \qquad \text{at } z = 0, \tag{4.5b}$$
$$\hat{v}_z = -\delta\left[1 - 2\beta - 2\delta\beta(1-\beta)C(\tau,\delta)\right]\hat{v} \qquad \text{at } z = h(\tau). \tag{4.5c}$$

We assume that the eigenvalues are ordered such that $\Re(\lambda_j) \geq \Re(\lambda_l)$ for $l > j$. To emphasise that the eigensolutions are parameterised by τ, we will occasionally write $\lambda = \lambda(\tau)$ and $v = v(z;\tau)$.

Let $(\mathcal{L}^*,\mathcal{B}^*)$ denote the adjoint of $(\mathcal{L},\mathcal{B})$ with respect to the standard inner production (which for two functions f_1 and f_2 is given by integrating $f_1\bar{f}_2$ with respect to z from 0 to $h(\tau)$, with the bar denoting complex conjugation) and let v_j^* be the adjoint eigenfunctions of $(\mathcal{L},\mathcal{B})$ i.e. the eigenfunctions of $(\mathcal{L}^*,\mathcal{B}^*)$ for the eigenvalues $\lambda = \lambda_j$. We impose the following normalisations,

$$\int_0^{h(\tau)} |v_j(z;\tau)|^2 dz = 1, \qquad \int_0^{h(\tau)} v_l^*(z;\tau)\bar{v}_j(z;\tau)dz = \delta_{jl}, \tag{4.6}$$

where the bar denotes complex conjugation and δ_{jl} is the Kronecker-symbol.

Inserting (4.4) into (4.3a) and then forming inner products with the adjoint eigenfunctions yields the ODE system

$$c_{l,t}(t) - \left(\lambda_l(\tau) + \delta\gamma_{ll}(\tau)\right)c_l(t) = \delta \sum_{j=1, j\neq l}^{N} \gamma_{lj}(\tau)c_j(t) \tag{4.7a}$$

with initial conditions

$$c_l(0) = c_{li} \equiv \int_0^1 v_l^*(z;0)\,\hat{c}_i(z)\,dz \tag{4.7b}$$

for $l = 1, 2, \ldots N$ and where

$$\gamma_{lj}(\tau) \equiv -\int_0^{h(\tau)} v_l^*(z;\tau)\,\bar{v}_{j,\tau}(z;\tau)\,dz. \tag{4.7c}$$

An alternative expression for the γ_{lj} with $j \neq l$ can be found by taking the derivative of (4.5a) with respect to τ for $\lambda = \lambda_j$ and forming the inner product with v_l^*, leading to

$$\gamma_{lj} = \frac{1}{\lambda_j - \lambda_l}\int_0^{h(\tau)} v_j^*(z)(\mathcal{L}_\tau \bar{v}_l)(z)\,dz. \tag{4.8}$$

For fixed τ and $\delta \to 0$, the operators $\mathcal{L}$ and $\mathcal{B}$ can be expanded as

$$\mathcal{L}(\tau,\delta) = \mathcal{L}_0(\tau) + \delta\mathcal{L}_1(\tau) + \cdots, \tag{4.9a}$$

$$\mathcal{B}(\tau,\delta) = \mathcal{B}_0(\tau) + \delta\mathcal{B}_1(\tau) + \cdots, \tag{4.9b}$$

where we will in particular need the leading order operators. The expansions start with $O(1)$ terms even though C is $O(\delta^{-1})$, see (3.6). In $\mathcal{B}$, this is offset by a factor of δ^2, and the leading term C_0 does not contribute to $\mathcal{L}$ at all since it does not depend on z (cf. (3.8)). From the expansion for $\mathcal{L}$ and (4.8) we can conclude that the γ_{lj} are $O(1)$ for $l \neq j$, thus ensuring that the equations in (4.7) are indeed only weakly coupled.

4.3. Multiple scales analysis. The presence of slow and fast time scales allows us to seek asymptotic expansions for the c_l using the "explicit" multiple scales method [23, 24], where the dependence on the slow time is fixed by eliminating secular terms from higher order corrections. The situation here differs slightly from the typical application of this method in that the leading order problem has solutions that decay or grow exponentially rather than being periodic. We will limit our derivation here to the case of two modes $N = 2$ and assume that these two modes are real; numerical inspection of the leading modes for $(\mathcal{L}, \mathcal{B})$ suggests that this is reasonable.

We begin by substituting the ansatz

$$c_j(t) = d_j(T)\exp\left(\beta_j(t)\right), \tag{4.10}$$

into (4.7) (truncated to two equations for c_1 and c_2), where

$$T \equiv \beta_1(t) - \beta_2(t) \tag{4.11}$$

is a new fast time, and

$$\beta_j(t) \equiv \int_0^{\delta t} \delta^{-1}\lambda_j(\rho)d\rho + \int_0^{\delta t} \gamma_{jj}(\rho)d\rho, \tag{4.12}$$

We obtain

$$d_{1,T}(T) = \frac{\delta\gamma_{12}(\tau)}{\lambda(\tau) + \delta\gamma(\tau)}\exp\left(-T\right)d_2(T), \tag{4.13a}$$

$$d_{2,T}(T) = \frac{\delta\gamma_{21}(\tau)}{\lambda(\tau) + \delta\gamma(\tau)}\exp\left(T\right)d_1(T), \tag{4.13b}$$

$$d_1(0) = c_{1i}, \qquad d_2(0) = c_{2i}, \tag{4.13c}$$

with $\lambda \equiv \lambda_1 - \lambda_2$ and $\gamma \equiv \gamma_{11} - \gamma_{22}$. Since the problem is linear, we may assume, without loss of generality, that (c_{1i}, c_{2i}) have a 2-norm of one, $(c_{1i}^2 + c_{2i}^2)^{1/2} = 1$. Also notice that the eigenvalues of $(\mathcal{L}, \mathcal{B})$ can be expanded as

$$\lambda(\tau) = \lambda^{(0)}(\tau) + \delta\lambda^{(1)}(\tau) + \delta^2\lambda^{(2)}(\tau) + \ldots, \tag{4.14}$$

and that similar expansions can be obtained for the (adjoint) eigenfunctions, the quantities γ, γ_{12}, γ_{21}, and the initial conditions c_{1i} and c_{2i}.

We now expand d_l as

$$d_1(T) = d_1^{(0)}(T,\tau) + \delta d_1^{(1)}(T,\tau) + \delta^2 d_1^{(2)}(T,\tau) + \ldots, \quad l = 1,2 \tag{4.15}$$

and the derivatives as

$$d_{l,T} = d_{l,T}^{(0)} + \delta\left(d_{l,T}^{(1)} + \frac{l}{\lambda^{(0)}} d_{l,\tau}^{(0)}\right) + \delta^2\left(d_{l,T}^{(2)} + \frac{l}{\lambda^{(0)}} d_{l,\tau}^{(1)} - \frac{\lambda^{(1)} + \gamma^{(0)}}{\left(\lambda^{(0)}\right)^2} d_{l,\tau}^{(0)}\right) + \ldots. \tag{4.16}$$

and consider the problems for the $d_l^{(n)}$ order by order.

To leading order, we find that $d_1^{(0)} = d_1^{(0)}(\tau)$ and $d_2^{(0)} = d_2^{(0)}(\tau)$ are independent of T and satisfy the initial conditions

$$d_1^{(0)}(0) = c_{1i}^{(0)} \quad \text{and} \quad d_2^{(0)}(0) = c_{2i}^{(0)}. \tag{4.17}$$

The functions $d_l^{(0)}(\tau)$, $l = 1,2$ are determined by considering the next order problem, which is

$$d_{1,T}^{(1)}(T,\tau) = \frac{\gamma_{12}^{(0)}(\tau)}{\lambda^{(0)}(\tau)} \exp(-T) d_2^{(0)}(\tau) - \frac{d_{1,\tau}^{(0)}(\tau)}{\lambda^{(0)}(\tau)}, \tag{4.18a}$$

$$d_{2,T}^{(1)}(T,\tau) = \frac{\gamma_{21}^{(0)}(\tau)}{\lambda^{(0)}(\tau)} \exp(T) d_1^{(0)}(\tau) - \frac{d_{2,\tau}^{(0)}(\tau)}{\lambda^{(0)}(\tau)}, \tag{4.18b}$$

$$d_1^{(1)}(0,0) = c_{1i}^{(1)}, \qquad d_2^{(1)}(0,0) = c_{2i}^{(1)}. \tag{4.18c}$$

The last terms in (4.18a) and (4.18b) are capable of introducing secular terms to the corrections and therefore need to be eliminated. This implies that $d_1^{(0)}$ and $d_2^{(0)}$ are also constant in τ, thus

$$d_1^{(0)} = c_{1i}^{(0)}, \qquad d_2^{(0)} = c_{2i}^{(0)}. \tag{4.19}$$

We wish to carry the approximation one order further and integrate (4.18), which introduces two new τ-dependent constants that are determined by eliminating secular terms from the second order correction problem. The details of this calculation are

given in the appendix. The result yields the following approximation for c_1 and c_2,

$$c_1(t) = c_{1i}^{(0)} \exp(\beta_1(t)) - \delta \frac{\gamma_{12}^{(0)}(\tau)}{\lambda^{(0)}(\tau)} \exp(\beta_2(t)) c_{2i}^{(0)} + \delta \left[c_{1i}^{(1)} + c_{1i}^{(0)} \int_0^\tau \frac{\gamma_{12}^{(0)}(\rho)\gamma_{21}^{(0)}(\rho)}{\lambda^{(0)}(\rho)} d\rho + \frac{\gamma_{12}^{(0)}(0)}{\lambda^{(0)}(0)} c_{2i}^{(0)} \right] \exp(\beta_1(t)), \tag{4.20a}$$

$$c_2(t) = c_{2i}^{(0)} \exp(\beta_2(t)) + \delta \frac{\gamma_{21}^{(0)}(\tau)}{\lambda^{(0)}(\tau)} \exp(\beta_1(t)) c_{1i}^{(0)} + \delta \left[c_{2i}^{(1)} + c_{2i}^{(0)} \int_0^\tau \frac{\gamma_{12}^{(0)}(\rho)\gamma_{21}^{(0)}(\rho)}{-\lambda^{(0)}(\rho)} d\rho + \frac{\gamma_{21}^{(0)}(0)}{-\lambda^{(0)}(0)} c_{1i}^{(0)} \right] \exp(\beta_2(t)). \tag{4.20b}$$

Notice that the $O(\delta)$ corrections in the coefficients of the exponentials in (4.21) are divided by the difference of the first and second eigenvalue. This emphasises the importance of maintaining an $O(1)$ gap between in particular these two eigenvalues as $\delta \to 0$; double or nearly double eigenvalues require a separate discussion. On the other hand, no restriction seems to be required for the individual eigenvalues, so that the approximation remains valid even near stability transitions, i.e. where $|\lambda_1|$ becomes small.

We can now insert (4.20) into the two mode truncation of (4.4) to obtain an approximation for $\hat{c}$. For $t \to \infty$, only the terms proportional to $\exp(\beta_1(t))$ survive, thus

$$\hat{c}(z,t) \approx \left\{ c_{1,i}^{(0)} v_1(z;\delta t) + \delta \left[c_{1i}^{(1)} + c_{1i}^{(0)} \int_0^{\delta t} \frac{\gamma_{12}^{(0)}(\rho)\gamma_{21}^{(0)}(\rho)}{\lambda^{(0)}(\rho)} d\rho + \frac{\gamma_{12}^{(0)}(0)}{\lambda^{(0)}(0)} c_{2i}^{(0)} \right] v_1(z;\delta t) + \delta c_{1,i}^{(0)} \frac{\gamma_{21}^{(0)}(\delta t)}{\lambda^{(0)}(\delta t)} v_2(z;\delta t) + O(\delta^2) \right\} \exp\left[\int_0^{\delta t} \delta^{-1}\lambda_1(\rho) + \gamma_{11}(\rho) d\rho \right]. \tag{4.21}$$

This result suggests a straightforward generalisation to the case with a general number of N modes,

$$\hat{c}(z,t) \approx \left\{ c_{1,i}^{(0)} v_1(z;\delta t) + \delta c_{1,i}^{(1)} v_1(z;\delta t) + \delta \sum_{l=2}^{N} \left[c_{1i}^{(0)} \int_0^{\delta t} \frac{\gamma_{1l}^{(0)}(\rho)\gamma_{l1}^{(0)}(\rho)}{\lambda_1^{(0)}(\rho) - \lambda_l^{(0)}(\rho)} d\rho + \frac{\gamma_{1l}^{(0)}(0)}{\lambda_1^{(0)}(0) - \lambda_l^{(0)}(0)} c_{li}^{(0)} \right] v_1(z;\delta t) + \delta c_{1i}^{(0)} \sum_{l=2}^{N} \frac{\gamma_{l1}^{(0)}(\delta t)}{\lambda_1^{(0)}(\delta t) - \lambda_l^{(0)}(\delta t)} v_l(z;\delta t) + O(\delta^2) \right\} \exp\left[\int_0^{\delta t} \delta^{-1}\lambda_1(\rho) + \gamma_{11}(\rho) d\rho \right]. \tag{4.22}$$

If we take $N \to \infty$, we see that the corrections remain small provided the two infinite series that arise in (4.22) converge (for fixed time). The terms in the first series have denominators that are the distance of the first eigenvalue from the l-th eigenvalue. Motivated by the theory for Sturm-Liouville problems, we would expect that $|\lambda_l| = O(l^2)$ for $l \to \infty$. Our numerical trials confirm that this is indeed the case for the eigenvalues of (4.5). Moreover, these trials suggest that the γ_{l1} remain bounded as l increases and therefore we can expect the first series to converge for appropriately normalised initial data $c_{li}^{(0)}$. A similar argument can be made for the second sum in (4.22) i.e. in the bottom line.

4.4. Comparison with numerical solutions. We now compare the asymptotic approximations obtained in the previous section with numerical solutions of (4.3). For this we introduce two ways to truncate (4.21) which approximate $\hat{c}$ with a different degree of accuracy. The first, or basic, approximation only retains the leading order in δ behaviour in all its constituents (exponents and prefactors),

$$\hat{c}_{\rm bas}(z,t) = c_{1i}^{(0)} v_1^{(0)}(z;\delta t) \exp\left[\int_0^{\delta t} \delta^{-1}\lambda_1^{(0)}(\rho) d\rho\right], \tag{4.23a}$$

$$c_{1i}^{(0)} = \int_0^1 v_1^{*(0)}(z;0)\,\hat{c}_i(z)\,dz, \tag{4.23b}$$

where ${v_1}^{(0)}$ and $v_1^{*(0)}$ is the leading order part of the δ-expansion for the first eigenfunction and for the first adjoint eigenfunction, respectively. The second, improved one uses the full eigenvalues and (adjoint) eigenfunctions of the operator $\mathcal{L}$ instead of the leading order approximations,

$$\hat{c}_{\rm imp}(z,t) = c_{1i} v_1(z;\delta t) \exp\left[\int_0^{\delta t} \delta^{-1}\lambda_1(\rho) + \gamma_{11}(\rho) d\rho\right], \tag{4.24a}$$

$$c_{1i} = \int_0^1 v_1^{*}(z;0)\,\hat{c}_i(z)\,dz. \tag{4.24b}$$

The approximation $\hat{c}_{\rm bas}$ has the advantage that the τ-dependence of the can be easily scaled out of the leading order eigenproblem. To see this, we return to the formulation (4.2) of the eigenproblem, take the leading order problem and rescale according to

$$z = h_0\,\check{z}, \quad \lambda^{(0)} = h_0^{-2}\,\check{\lambda}, \quad k = h_0^{-1}\check{k}, \quad \hat{c}^{(0)} = \check{c},$$
$$\hat{p}^{(0)} = \frac{\beta h_0^{-1}\check{p}}{h_0 - 1 + \beta}, \quad \hat{w}^{(0)} = \frac{\beta\check{w}}{h_0 - 1 + \beta}, \quad \mathcal{M} = \frac{h_0 - 1 + \beta}{\beta}\,{\rm Ma}. \tag{4.25}$$

As a result, we obtain the following equations in the bulk,

$$\check{p}_{\check{z}\check{z}} - \check{k}^2\check{p} = 0, \qquad \check{w}_{\check{z}\check{z}} - \check{k}^2\check{w} = \check{p}_{\check{z}}, \qquad \check{\lambda}\check{c} - \check{z}\check{w} = \check{c}_{\check{z}\check{z}} - \check{k}^2\check{c}, \tag{4.26a}$$

and the boundary conditions

$$\check{w} = 0, \quad \check{w}_z = 0, \quad \check{c}_z = 0, \qquad \text{at } \check{z} = 0 \tag{4.26b}$$

$$\check{w} = 0, \quad \check{c}_z = 0, \quad \check{p}_z = -\check{k}^2\,\mathcal{M}\,\check{c}, \qquad \text{at } \check{z} = 1. \tag{4.26c}$$

As τ changes, $\check{k}$ and $\mathcal{M}$ change if k and Ma are kept fixed, so we need to solve (4.26) for all values of $\check{k}$ and $\mathcal{M}$. If we use the notation $\check{\lambda}_1 = \check{\lambda}_1(\check{k},\mathcal{M})$ and $\check{v}_1 = \check{v}_1(\check{z};\check{k},\mathcal{M})$ to make the dependence of the eigensolution (here for the top eigenvalue and eigenfunction) on $\check{k}$ and $\mathcal{M}$ explicit, we can express $\lambda_1^{(0)}$ and $v_1^{(0)}(z;\tau)$ as

$$\lambda_1^{(0)}(\tau) = h_0(\tau)^{-2}\check{\lambda}_1\left(h_0(\tau)k, \frac{h_0 - 1 + \beta}{\beta}\,{\rm Ma}\right), \tag{4.27a}$$

$$v_1^{(0)}(z;\tau) = \check{v}_1\left(\frac{z}{h_0(\tau)}; h_0(\tau)k, \frac{h_0 - 1 + \beta}{\beta}\,{\rm Ma}\right), \tag{4.27b}$$

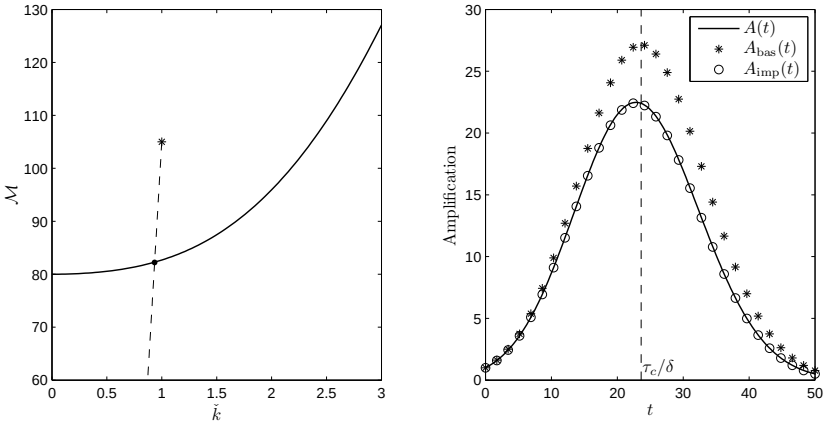

FIG. 4.1. *(a), left: Regions where the top eigenvalue of the leading order part of the operator $\mathcal{L}$ are positive or negative (above and below the solid line). The dashed line shows the values of $\check{k}$ and $\mathcal{M}$ that are traversed for the fixed values of k and Ma used by the numerical computations* (4.32). *The star emphasises the initial value for $\check{k}$ and $\mathcal{M}$ and the bullet denotes the intersection with the boundary between the two regions. Further explanations are given in the text. (b), right: Comparison of the amplification obtained for the numerical solution of the exact linearized problem with those for the asymptotic approximations. The initial perturbation was the eigenfunction associated with the top eigenvalue for $\mathcal{L}$ at $\tau = 0$. Further explanations including the definition of the amplifications are given in the text.*

and then use these in (4.23). After that we can eliminate the dependence on $h_0(\tau)$ from the integrand in the exponential by choosing $\eta = h_0$ as the new integration variable, so that

$$c_{\rm bas}(z,t) = c_{1i}^{(0)} v_1^{(0)}(z;\tau) \exp\left(I/\delta\right), \quad I = \int_{h_0(\tau)}^{1} \frac{\check{\lambda}_1\left(\eta k, \frac{\eta-1+\beta}{\beta}\,\mathrm{Ma}\right)}{\eta(\eta-1+\beta)} d\eta. \tag{4.28}$$

We now collect some properties of (4.26). The problem corresponds to the insulating case in Pearson's work [34] on thermal Bénard-Marangoni convection. An argument by Lin [27] can be used to show that the spectrum of this problem consists exclusively of discrete eigenvalues $\check{\lambda}$. Vrentas and Vrentas [46] proved that when an eigenvalue crosses a stability boundary its real part changes sign and the imaginary part vanishes. Furthermore, we numerically inspected the top ten eigenvalues $\check{\lambda}_n$ (ordered according to their real part) for a range of wavenumbers $\check{k}$ and Marangoni-numbers $\mathcal{M}$. These eigenvalues were always real, i.e. the imaginary part was numerically zero, and the behaviour for large n was found to be $\lambda_n^{(0)} = O(n^2)$. The eigenvalues appeared to remain separated for all values of $\mathcal{M}$ and $\check{k}$ we inspected. For the full eigenproblem (i.e. for $(\mathcal{L},\mathcal{B})$) these properties can either be inferred by perturbation arguments or probed for plausibility by numerical computations.

Returning to the leading order eigenproblem, fig. 4.1(a) describes the situation for the top eigenvalue $\check{\lambda}_1$ in the $(\check{k},\mathcal{M})$ plane. The plane is split into two regions where $\check{\lambda}_1$ is either positive or negative; the line separating the two regions represents the cut-off wave number $\check{k}_{\rm cut}(\mathcal{M})$ for each value of $\mathcal{M}$ and is characterised by the condition that $\check{\lambda}_1$ is zero there. Above the line, the eigenvalue is positive, and below, it is negative; it ends at $\check{k} = 0$ at the critical Marangoni-number $\mathcal{M}_c$. The value

for $\mathcal{M}_c$ can be found from a small k expansion to be $\mathcal{M}_c = 80$. The implication is that for each $\mathcal{M} > \mathcal{M}_c$, the top eigenvalue is positive for a range of wave numbers $0 < \check{k} < \check{k}_{\rm cut}$ and negative for larger $\check{k}$. We remark in passing that for fixed $\mathcal{M}$, the eigenvalue achieves its largest positive value for a wavenumber $\check{k}_m$ that by numerical inspection is found to be typically order one or larger except if $\mathcal{M}$ is (very) close to $\mathcal{M}_c$. For Marangoni numbers below $\mathcal{M}_c$, all eigenvalues are negative.

Our goal is to compare the approximations (4.23) and (4.24) with numerical solutions for (4.3) by choosing an initial perturbation and then comparing the amplification that is achieved. For the numerical solution and each of approximations, the amplification is defined by

$$A(t) = \frac{\max_z |\hat{c}(z,t)|}{\max_z |\hat{c}(z,0)|}, \quad A_{\rm bas}(t) = \frac{\max_z |\hat{c}_{\rm bas}(z,t)|}{\max_z |\hat{c}(z,0)|}, \quad A_{\rm imp}(t) = \frac{\max_z |\hat{c}_{\rm imp}(z,t)|}{\max_z |\hat{c}(z,0)|}, \tag{4.29}$$

respectively. Note that the denominator is the same in all three expressions; as a result, the initial amplification does not need to be one for $A_{\rm bas}$ and $A_{\rm imp}$. From (4.23a) and (4.24) we obtain

$$A_{\rm bas}(t) = |c_{1i}^{(0)}| \frac{\max_z |v_1^{(0)}(z;\tau)|}{\max_z |\hat{c}(z,0)|} \exp\left[\int_0^{\delta t} \delta^{-1} \lambda_1^{(0)}(\rho) d\rho\right], \tag{4.30a}$$

$$A_{\rm imp}(t) = |c_{1i}| \frac{\max_z |v_1(z;\tau)|}{\max_z |\hat{c}(z,0)|} \exp\left[\int_0^{\delta t} \delta^{-1} \lambda_1(\rho) + \gamma_{11}(\rho) d\rho\right]. \tag{4.30b}$$

For our first set of comparisons, we pick the eigenfunction of the top eigenvalue for the full operator $\mathcal{L}$ with $\tau = 0$ as initial condition,

$$\hat{c}_i(z) = \frac{v_1(z;0)}{\max_z |v_1(z;0)|}, \tag{4.31}$$

which we have normalised here with respect to the maximum norm for definiteness. For (4.31), c_{1i} and $c_{1i}^{(0)}$ are equal to one and c_{2i} and $c_{2i}^{(0)}$ are zero.

For the numerical solution of the linearised system (4.3) and also for the asymptotic results, we use the long time approximation (3.6) of the base state retaining the first two terms for C and the leading order term for h, with $C_1(0,\tau)$ in (3.12) set to zero. The resulting operator $(\mathcal{L}, \mathcal{B})$ is only correct to leading order but for comparing the results of the three solutions/approximations it is sufficient to be consistent and use the same base state for all of them.

Furthermore, we use the following parameters

$$\delta = 0.01, \qquad \beta = 0.3, \qquad {\rm Ma} = 105, \qquad k = 1. \tag{4.32}$$

The path described by $\check{k}$ and $\mathcal{M}$ in the ($\check{k}$,$\mathcal{M}$) plane for these values of k and Ma as the base state slowly changes is indicated in 4.1(a) by a dashed line, with the initial value $(k, {\rm Ma})$ indicated by a star. The point where the line intersects the line $\check{\lambda} = 0$ is emphasised by a bullet; let τ_c denote the value of the slow time variable at which this happens. For $\tau < \tau_c$, the exponential factor in (4.23a) grows and it decays for $\tau > \tau_c$, as shown in fig. (4.1)(b). This is in good agreement with the time at which $A_{\rm imp}$ and A achieve their maximum. Also, the magnitudes of the amplifications agree reasonably well, and in fact the improved asymptotic and the numerical result nearly coincide.

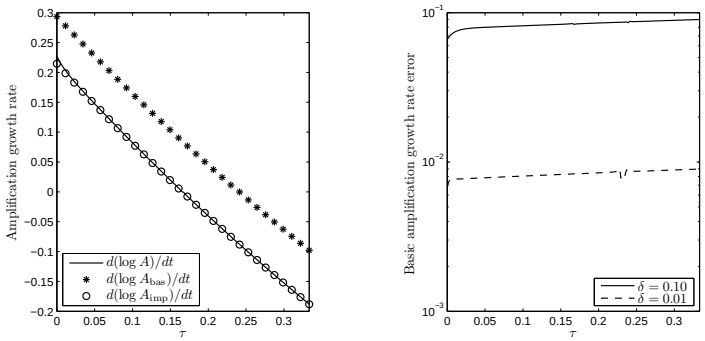

FIG. 4.2. *(a), left: Comparison of the growth rate of the log of the three types of amplifications defined in* (4.29)*, for* $\delta = 0.1$*. (b), right: The absolute value of the difference between the growth rate of the log of A and the basic asymptotic approximation* A_{bas}*, for two different values of* δ*.*

For closer verification of our asymptotic results, we compare the time derivative of the log of A, $A_{\rm bas}$ and $A_{\rm imp}$. In fig. 4.2(a), we chose a value of $\delta = 0.1$ that is considerably larger than previously, because otherwise the lines would be hard to distinguish on the scale of the figure. At this value of δ, $d\log(A(t))/dt$ agrees moderately well with $d\log(A_{\rm bas}(t))/dt$ and very well with $d\log(A_{\rm imp}(t))/dt$. From (4.30) and (4.21), we find that the difference of the growth rates for the numerical and basic amplifications, $d\log(A/A_{\rm bas}(t))/dt$, is $O(\delta)$ for $\delta \to 0$ (with τ fixed), and this is confirmed by fig. 4.2(b) where the values decrease by a factor of ten as δ is lowered from 0.1 to 0.01.

Next we consider the projection onto the eigensolutions and compare

$$c_j(t) = \int_0^{h(\tau)} v_j^*(z;\tau)\,\hat{c}(z,\tau)\,dz$$

with

$$c_1(t) = \left\{1 + \delta \int_0^{\delta t} \frac{\gamma_{12}(\rho)\gamma_{21}(\rho)}{\lambda(\rho)} d\rho\right\} \exp\left[\int_0^{\delta t} \delta^{-1}\lambda_1(\rho) + \gamma_{11}(\rho) d\rho\right], \tag{4.33a}$$

$$\begin{aligned} c_2(t) = {} & \delta \frac{\gamma_{21}(\tau)}{\lambda(\tau)} \exp\left[\int_0^{\delta t} \delta^{-1}\lambda_1(\rho) + \gamma_{11}(\rho) d\rho\right] \\ & - \delta \frac{\gamma_{21}(0)}{\lambda(0)} \exp\left[\int_0^{\delta t} \delta^{-1}\lambda_2(\rho) + \gamma_{22}(\rho) d\rho\right]. \end{aligned} \tag{4.33b}$$

The graphs coincide perfectly in fig. 4.3 thus verifying in particular the $O(\delta)$ contribution to c_2.

We now turn to more generic initial data for the perturbation

$$c_i(z) = 16z^2(1-z)^2; \tag{4.34}$$

when we compute the numerical solution for $\hat{c}$ from (4.3). We show the results for two different base states: the asymptotic approximation for the long time base state used previously in this section and a numerical solution of (3.1) with well-mixed initial conditions $C(z,0) = 0$. The latter base state differs from the former mainly at early

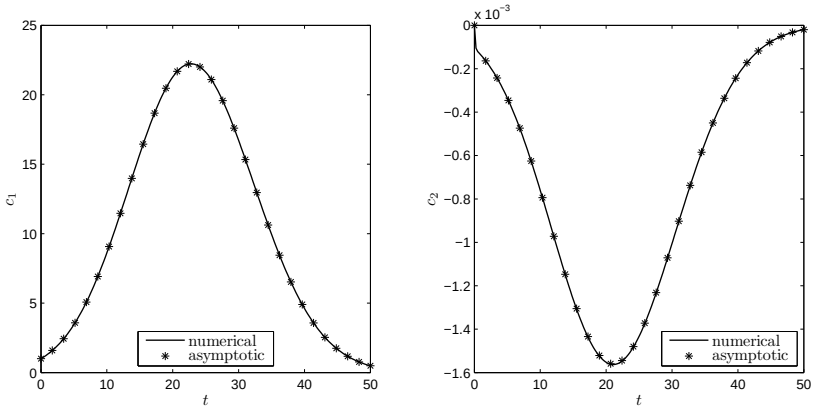

FIG. 4.3. *Comparison of the projections c_1 (left) and c_2 (right) of the numerical solution* (4.3) *with the asymptotic expressions presented in* (4.33).

times where it has a rapidly evolving boundary layer which the former does not. The wave and Marangoni-numbers k and Ma are the same as before.

Fig. 4.4 (a) shows a comparison of the asymptotic amplifications. The results obtained from solutions of (3.1) are labelled "(num)" or "(asy)", respectively, if the numerical solution or the asymptotic approximation for the base state is used. The best agreement is achieved between the improved asymptotic amplification $A_{\rm imp}$ and the numerical solution with the asymptotic base state "$A(t)$ (asy)". The amplifications for the basic approximation is visibly different since it only uses the leading order approximation for the eigenvalue $\lambda_1^{(0)}$. There is also a discrepancy between the "$A(t)$ (asy)" and "$A(t)$ (num)" which reflects the influence of the rapidly evolving boundary layer in the base state.

The initial perturbation (4.34) is not a pure eigenfunction thus several $c_l(0)$ (cf. (4.7b)) are non-zero and not even close to zero. All contributions for the sub-dominant modes decay rapidly compared to the one for the top mode, however, so that therefore the improved asymptotic approximation and the "$A(t)$ (asy)" agree very well except perhaps at early times. The effect of the higher modes is perhaps best seen if we compare asymptotic and numerical growth rates, rather than amplifications, in fig. 4.4 (b). At later times, $\lambda_1 = d(\log(A_{\rm bas}))/dt$ and (in fact, both) numerical growth rates agree very well - the difference is $O(\delta)$ and does not show up as well as in the amplifications on the left where the error is accumulated in time. At early times, however, the asymptotic growth rate differs from the numerical ones.

Including contributions from subdominant eigenvalues via

$$A_N(t) = \frac{\max_z |\hat{c}_{{\rm bas},N}(z,t)|}{\max_z |\hat{c}(z,0)|}. \tag{4.35}$$

where

$$\hat{c}_{{\rm bas},N}(z,t) = \sum_{k=1}^{N} c_{ki}^{(0)} v_k^{(0)}(z,\tau) \exp\left[\delta^{-1} \int_0^{\delta t} \lambda_k^{(0)}(\rho)\, d\rho\right],$$
$$c_{ki}^{(0)} = \int_0^1 v_k^{*(0)}(z;0)\, \hat{c}_i(z)\, dz.$$

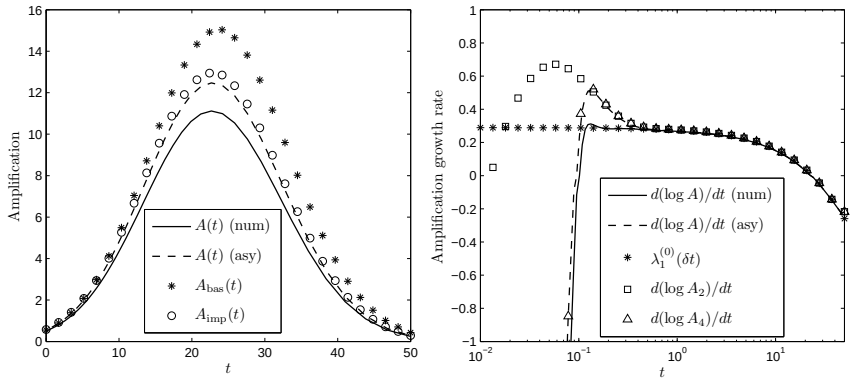

FIG. 4.4. *(a), left: A comparison of the asymptotic amplifications with the ones obtained from numerical solutions of* (4.3)*. The difference between "A(t) (asy)" and "A(t) (num)" is explained in the text. (b), right: Comparison of the growth rates i.e. the derivative of the log of the amplifications. Shown are the lines for the growth rates obtained from "A(t) (asy)" and "A(t) (num)", from the basic asymptotic approximation and from the approximations A_N (cf.* (4.35)*) using two and four modes.*

reduces this difference. For $N \geq 4$, the growth rates derived from A_N agree very well with the numerical growth rate "$d(\log(A))/dt$ (asy)" even at early times, where the label "(asy)" has the same meaning as in fig. 4.4 (a).

5. Comparison with experiments. We now compare our results to some recent experiments by Bassou and Rharbi [1] using solutions of polystyrene (PS) with a molecular weight of 150 kg/mol in toluene. The mixture was deposited on a glass substrate and then dried in a chamber which was kept at a uniform temperature. The film was observed during the drying process by a variety of visualisation techniques to allow for the detection and measurement of convection cells.

The chamber was fitted with lids having holes of different sizes so that the evaporation rate could be controlled. The authors determined the drying rate J by measuring the mass loss of the experiment, and then dividing the measured value by time and the total surface area of the film. Thus, their drying rate corresponds to the right hand side of (2.5). Specifically, we can set the value J they measure in the first 30 seconds of their experiment approximately equal to the initial value of the right hand side of (2.5), i.e. $J = k_m c_m$. Expressing δ in terms of J, we get

$$\delta = \frac{J h_i}{D c_m}, \qquad c_m = \beta \rho. \tag{5.1}$$

For the majority of their reported results, the initial drying rate is $3 \times 10^{-4}\,\mathrm{kg/m^2\ s}$ and the volume fraction $\beta = 0.85$; h_i is between 1.4 and 0.15 mm. We follow Bassou and Rharbi and obtain the diffusion constant from measurements by Nanagara et al. [32], although those were carried out for PS with a larger molecular weight. The diffusivity depends on the volume fraction and by interpolating the data curves we obtain $D = 1.38 \times 10^{-9}\ \mathrm{m^2/s}$ for $\beta = 0.85$. PS and toluene both have a density close to 1000 $\mathrm{kg/m^3}$, so our assumption of a constant density for the liquid mixture seems justified, and we will use the aforementioned value for ρ. We thus have for the thickest film $\delta = 0.36$ and for the thinnest $\delta = 3.8 \times 10^{-2}$ so that we can assume $\delta \ll 1$.

To assess the stability of the liquid film, we also need the Marangoni-number Ma introduced in the previous section. Replacing the factor of δ by (5.1) yields

$$\mathrm{Ma} = \frac{(1-\beta)\gamma_c J {h_i}^2}{\mu D^2}. \tag{5.2}$$

The dependence of the surface tension coefficient on the composition of the liquid mixture was measured by Bassou and Rharbi and the resulting γ_c was found to be 8.5×10^{-7} (N/m)/(mol/m^3). The molar mass of toluene is 92.1×10^{-3} kg/mol, thus $\gamma_c = 9.2 \times 10^{-6}$ (N/m)/(kg/m^3). The viscosity was given for a number of polystyrene concentrations, and for $\beta = 0.85$ it was $\mu = 0.15$ Pa·s. For the largest initial film thickness $h_i = 1.4$ mm, the Marangoni number is then $\mathcal{M} = 2.9 \times 10^3$ and for the thinnest films $h_i = 0.15$ mm, we obtain $\mathcal{M} = 33$. Thus the top eigenvalue of the leading order part of $\mathcal{L}$ suggests that the solutions of (4.3) have a positive growth at least initially for a range of wave numbers, but for the thinner ones they always decay. The critical initial thickness where $\mathcal{M} = \mathcal{M}_c$ is found to be 0.23 mm. While the prediction agrees with the experimental observations for the thicker films, the thinner films in the experiments were unstable down to 0.15 mm; indications of stabilisation were only seen for $h_i \leq 0.1$ mm.

Next we consider the amplification of the perturbation, starting with the experiments with the largest initial film thicknesses. For $\mathcal{M} = 2.9 \times 10^3$, the maximum initial growth rate assuming a fully developed base state is given by the top eigenvalue of $\mathcal{L}_0$ for $k_m = 7.2$ and is $\lambda_m = 2.3 \times 10^2$. To gain three orders of magnitude at this growth rate the perturbation requires a dimensionless time of $t = 3.0 \times 10^{-2} \ll 1$. This contradicts the assumption of a fully developed base state but suggests that the instability will grow very quickly, even before the concentration boundary layer has fully penetrated the film.

To get into a situation where our theory applies for reasonable initial perturbations, we need to look at situations where the top eigenvalue is smaller, i.e. closer to criticality. In the experiment, this is achieved, for example, by reducing the initial film thickness. In fact, as noted before, the smaller film thicknesses used by Bassou and Rharbi correspond to Marangoni-numbers near to or even below $\mathcal{M}_c$.

To measure how far we are above criticality, we define

$$\varepsilon(\tau) \equiv \frac{\mathcal{M}(\tau) - \mathcal{M}_c}{\mathcal{M}_c}, \qquad \varepsilon_0 \equiv \varepsilon(0) = \frac{\mathrm{Ma} - \mathcal{M}_c}{\mathcal{M}_c}, \tag{5.3}$$

where $\mathcal{M}$ is given by (4.25) for a fixed choice of Ma; recall that $\mathcal{M}(0)$=Ma. Here we have emphasised the dependence of both the Marangoni-number and of ε on the slow time τ.

Next we expand the eigenvalue $\check{\lambda}_1$ in a Taylor series in terms of $\check{k}$,

$$\check{\lambda}_1 = \varepsilon \check{k}^2 + \left(-\frac{8}{315} + \frac{29}{630}\,\varepsilon + \frac{1}{14}\,\varepsilon^2 \right) \check{k}^4 + O(\check{k}^6). \tag{5.4}$$

By experimentation, we found that for the range of ε we use here, the series converges reasonably fast for k smaller than about 1.5. From this expansion, we find the following initial leading order behaviour for the cut-off and dominant wavenumber as well as the maximum growth rate, valid for $\varepsilon_0 \ll 1$,

$$\check{k}_c = \frac{3\sqrt{70}}{4}\,\varepsilon_0^{1/2}, \qquad \check{k}_m = \frac{3\sqrt{35}}{4}\,\varepsilon_0^{1/2}, \qquad \check{\lambda}_{1m} = \frac{315}{32}\,\varepsilon_0^2, \tag{5.5}$$

respectively. An obvious choice for the initial ε_0 and thus the Marangoni-number would be to let $\varepsilon_0 = \delta^{1/2}$, so that $\check{\lambda}_{1m} = O(\delta)$ in the beginning. However, the eigenvalue will change its sign as the line $\check{\lambda}_1 = 0$ is approached, and this happens so quickly that the amplification achieved at this time very small. Moreover, if $\check{\lambda}_1 = O(\delta)$, then $\check{\lambda}_1/\delta$ is of the same order as the terms neglected in the integral I for c_{bas} (cf. (4.28)) making estimates of the maximum amplification inaccurate. (Note, however, that our arguments here rely on orders of magnitude of the amplification, which will be small in this situation with our without higher corrections to I). Therefore, we will consider $\varepsilon_0 \gg \delta^{1/2}$.

We determine the amplification by evaluating, for fixed k and Ma, the integral I in (4.28). Letting $\varepsilon = (1 + (\eta - 1)/\beta)(1 + \varepsilon_0) - 1$ and $\check{k} = \eta k$ in (5.4) (with enough terms to ensure accuracy), we obtain an expression that can be plugged into I. In principle, this yields an explicit result but the algebra and resulting expressions are tedious and were handled by using Maple. We therefore only report the numerical results for a couple of specific choices of parameters. As before, we use $\beta = 0.85$.

We start with a small value for $\varepsilon_0 = 0.1$ and $k = 1.0$. As expected, I first increases as the thickness $h_0 < 1$ decreases until it reaches a maximum of $I = 2.2 \times 10^{-3}$ after which it decays and eventually becomes negative. Other choices of k produced values for I that were equal or less than this value. The amplification that results from this is $\exp(I/\delta)$. If we assume that we need at least three orders of magnitude to amplify a perturbation so that it becomes visible in an experiment, we find that $\delta < 2.2 \times 10^{-3}/7 \approx 3 \times 10^{-4}$. Even if we relax our assumption and consider a factor of ten to be enough to create a visible pattern, this increases δ only by a factor of three which is still less than even the smallest δ reported by Bassou and Rharbi. Thus it seems unlikely that visible convection cells will show up.

These values have also been verified by solving the eigenvalue problem and the full linear problem numerically. More specifically, the top eigenvalue $\check{\lambda}_1$ was computed for various values of the film thickness and the integral I was evaluated using Gaussian quadrature. The maximum value was found to be $I = 2.2 \times 10^{-3}$, in accordance with the above result. Moreover, the corresponding amplification at this critical thickness and when $\delta = 3 \times 10^{-4}$ was found to be $A_{\text{bas}} = 1.6 \times 10^3$. This is of the same order of magnitude as the predicted amplification; the difference being a result of neglecting the prefactors in (4.28). Because of the time-dependence of the top eigenfunction in (4.28), the time at which the maximum amplification occurs does not coincide exactly with the time when I attains its maximum. However, we find that the maximum amplification actually matches A_{bas}, that is, $\max_t A(t) = 1.6 \times 10^3$.

Repeating the investigation with $\varepsilon_0 = 0.5$ (i.e. Ma = 120) and $k = 1.5$, we obtain $I = 0.15$. This matches the numerical value of I that is computed using the procedure described above. A sufficient amplification of three orders of magnitude would require $\delta < 0.02$. An initial Marangoni number of 120 is achieved with a film thickness of 0.287 mm and for this thickness, $\delta = 0.073$, well above the permissible value. The amplification achieved for this δ would be only about $\exp(0.15/0.073) < 10$, making it again unlikely that any manifestation of the instability can be seen even though the initial Ma is 50% above $\mathcal{M}_c$. Numerical simulations support these claims. The amplifications that are achieved when $\delta = 0.02$ are $A_c = \max_t A(t) = 2.4 \times 10^3$, where A_c denotes the amplification when I attains its maximum. When $\delta = 0.073$, we find $A_c = \max_t A(t) = 11$. All of these values are of the same order of magnitude as the predicted amplifications.

The expansion in (5.4) fails to converge for $\varepsilon_0 = 0.50$ and $k > 3/2$. Therefore, we

use numerical solutions to study the amplification of perturbations with wavenumbers that are larger than this value. We find that the maximum value of I over all of the wavenumbers is $\max_k I(k) = 0.17$, which is achieved when $k = 1.80$. Since these optimal values are close to values of k and I from the last paragraph, we conclude that the previous discussion is representative of dynamics when $\mathrm{Ma} = 120$.

In summary, the theory predicts more stable films than is actually observed in the experiments, so we need to revisit our model which may be too simple. Perhaps the strongest assumption that has been made is that of the system being isothermal. That is, temperature variations in the fluid have been neglected. It is well known, however, that the evaporation of solvent will lead to a cooling of the air-liquid interface, thus inducing a temperature gradient in the fluid. This, in turn, can lead to the onset of convection rolls through thermal buoyancy-driven and thermocapillary-driven instabilities. Preliminary estimates of the relevant dimensionless numbers suggest that while thermal buoyancy-driven convection can very likely be ruled out, in accordance with Bassou and Rharbi's own findings, the contribution from thermal Marangoni effects needs further investigation.

6. Conclusions. In this paper, we have investigated the stability of a thin layer of a mixture that is composed of a volatile solvent and a non-volatile polymer. The evaporation of the solvent induces a concentration gradient which in turn leads to Marangoni stresses that can drive a Bénard-Marangoni type instability if the surface tension at the liquid/gas interface increases with the polymer concentration. For a simplified model, we determine the base state and the linearise about this base state to determine its stability.

In contrast to classical Bénard-Marangoni convection, where the liquid layer is heated from below and the Marangoni stresses arise from the temperature dependence of surface tension, the base state is itself time dependent since the loss of solvent leads to a slow change in the film thickness and composition. Thus, the linearised system is not autonomous. We address this issue by first projecting the initial value problem onto the leading eigenmodes and then deriving multiple scales expansions for the solution of the resulting ODE system. These make use of the fact that the evaporation is slow on the diffusive time scale which governs the potential instability, encapsulated by a small Biot number δ. We determine both the leading order result and the first correction. The latter reveals that a necessary condition for the validity of the expansions is that the eigenvalues of the spatial operator remain well separated. We expect that a sufficient distance of the top eigenvalue from the rest of the spectrum is particularly important. On the other hand, the absolute value of the eigenvalues is not relevant for the validity of the expansions.

From the multiple scales expansions, we derive two approximations for the amplification of the top mode contribution to an initial perturbation (noticing that the subdominant modes will be irrelevant for all but very early times). The first, or basic, approximation only uses the leading order (in δ) part of all the contributions in the expansions. Thus, the argument of the exponential factor only contains the leading order approximation to the eigenvalue. The second uses in particular the full eigenvalue and also includes the "self-coupling" term γ_{11}. Comparison with numerical solutions of the full linearised initial value problem show that both approximations capture the evolution if δ is small enough.

The improved approximation is substantially more accurate than the basic one, but the latter is more readily obtained, so we rely on it to investigate the experiments by Bassou and Rharbi. Specifically, we use it to predict the maximum amplification

a perturbation achieves before the system restabilizes. It turns out that only very modest amplifications are achieved unless the initial Marangoni number is more than 50% above the critical Marangoni number $\mathcal{M}_c = 80$ obtained from the leading oder in δ operator.

Appendix.

In this appendix, we identify and solve the solvability condition that is required to fully determine the first order corrections $d_1^{(1)}$ and $d_2^{(1)}$. We first integrate (4.18),

$$d_1^{(1)}(T,\tau) = -\frac{\gamma_{12}^{(0)}(\tau)}{\lambda^{(0)}(\tau)}\exp(-T)c_{2i}^{(0)} + a_1(\tau), \tag{A.1a}$$

$$d_2^{(1)}(T,\tau) = \frac{\gamma_{21}^{(0)}(\tau)}{\lambda^{(0)}(\tau)}\exp(T)c_{1i}^{(0)} + a_2(\tau). \tag{A.1b}$$

The ODE system for the second order correction problem is

$$\begin{aligned} d_{1,T}^{(2)}(T,\tau) = {} & \frac{\gamma_{12}^{(0)}(\tau)}{\lambda^{(0)}(\tau)}\exp(-T)d_2^{(1)}(T,\tau) \\ & + \left[\frac{\gamma_{12}^{(1)}(\tau)}{\lambda^{(0)}(\tau)} - \frac{\gamma_{12}^{(0)}(\tau)}{(\lambda^{(0)}(\tau))^2}\left(\lambda^{(1)}(\tau)+\gamma^{(0)}(\tau)\right)\right]\exp(-T)d_2^{(0)}(\tau) \\ & - \frac{d_{1,\tau}^{(1)}(\tau)}{\lambda^{(0)}(\tau)}, \end{aligned} \tag{A.2a}$$

$$\begin{aligned} d_{2,T}^{(2)}(T,\tau) = {} & \frac{\gamma_{21}^{(0)}(\tau)}{\lambda^{(0)}(\tau)}\exp(T)d_1^{(1)}(T,\tau) \\ & + \left[\frac{\gamma_{21}^{(1)}(\tau)}{\lambda^{(0)}(\tau)} - \frac{\gamma_{21}^{(0)}(\tau)}{(\lambda^{(0)}(\tau))^2}\left(\lambda^{(1)}(\tau)+\gamma^{(0)}(\tau)\right)\right]\exp(T)d_1^{(0)}(\tau) \\ & - \frac{d_{2,\tau}^{(1)}(\tau)}{\lambda^{(0)}(\tau)}. \end{aligned} \tag{A.2b}$$

Inserting (4.19) and (A.1) into (A.2) and identifying the terms that may lead to secular terms yields the solvability condition

$$a_{1,\tau} = \frac{\gamma_{12}^{(0)}(\tau)\gamma_{21}^{(0)}(\tau)}{\lambda^{(0)}(\tau)}c_{1i}^{(0)}, \qquad a_{2,\tau} = -\frac{\gamma_{12}^{(0)}(\tau)\gamma_{21}^{(0)}(\tau)}{\lambda^{(0)}(\tau)}c_{2i}^{(0)}, \tag{A.3a}$$

with initial conditions arising from (4.18c),

$$a_1(0) = \frac{\gamma_{12}^{(0)}(0)}{\lambda^{(0)}(0)}c_{2i}^{(0)} + c_{1i}^{(1)}, \qquad a_2(0) = -\frac{\gamma_{21}^{(0)}(0)}{\lambda^{(0)}(0)}c_{1i}^{(0)} + c_{2i}^{(1)}. \tag{A.3b}$$

We solve these equations for a_1 and a_2 and insert the result into (A.1),

$$d_1^{(1)}(T,\tau) = -\frac{\gamma_{12}^{(0)}(\tau)}{\lambda^{(0)}(\tau)}\exp(-T)c_{2i}^{(0)} + c_{1i}^{(0)}\int_0^\tau \frac{\gamma_{12}^{(0)}(\rho)\gamma_{21}^{(0)}(\rho)}{\lambda^{(0)}(\rho)}d\rho + \frac{\gamma_{12}^{(0)}(0)}{\lambda^{(0)}(0)}c_{2i}^{(0)} + c_{1i}^{(1)}, \tag{A.4a}$$

$$d_2^{(1)}(T,\tau) = \frac{\gamma_{21}^{(0)}(\tau)}{\lambda^{(0)}(\tau)}\exp(T)c_{1i}^{(0)} - c_{2i}^{(0)}\int_0^\tau \frac{\gamma_{12}^{(0)}(\rho)\gamma_{21}^{(0)}(\rho)}{\lambda^{(0)}(\rho)}d\rho - \frac{\gamma_{21}^{(0)}(0)}{\lambda^{(0)}(0)}c_{1i}^{(0)} + c_{2i}^{(1)}. \tag{A.4b}$$

REFERENCES

[1] N. Bassou and Y. Rharbi, *Role of Bénard-Marangoni instabilities during solvent evaporation in polymer surface corrugations*, Langmuir, 25 (2009), pp. 624–632.

[2] H. Bénard, *Les tourbillons cellulaires dans une nappe liquide*, Revue Générale des Sciences, 11 (1900), pp. 1261–1271, 1309–1328.

[3] ———, *Les tourbillons cellulaires dans une nappe liquide transportent de la chaleur par convection en régime permanent*, Annales de Chimie Physique, 7 (1900), p. 62.

[4] ———, *Les tourbillons cellulaires dans une nappe liquide: Méthodes optiques d'observation et d'enregistrement*, Journal de Physique Théorique et Appliquée, 10 (1901), p. 254.

[5] B. S. Bhadauria and P. K. Bhatia, *Time-periodic heating of Rayleigh-Benard convection*, Physica Scripta, 66 (2002), pp. 59–65.

[6] M. J. Block, *Surface tension as the cause of Bénard cells and surface deformation in a liquid film.*, Nature, 178 (1956), pp. 650–651.

[7] E. Bodenschatz, W. Pesch, and G. Ahlers, *Recent developments in Rayleigh-Bénard convection*, Annual Review of Fluid Mechanics, 32 (2000), pp. 709–778.

[8] E. Bormashenko, S. Balter, R. Pogreb, Y. Bormashenko, O. Gendelman, and D. Aurbach, *On the mechanism of patterning in rapidly evaporated polymer solutions: Is temperature-gradient-driven marangoni instability responsible for the large-scale patterning?*, Journal of colloid and interface science, 343 (2010), p. 602–607.

[9] D. E. Bornside, C. W. Macosko, and L. E. Scriven, *Spin coating: One-dimensional model*, Journal of Applied Physics, 66 (1989), pp. 5185–5193.

[10] M. Bouthier, *Stabilité linéaire des écoulements presque parallèlles*, Journal de Mécanique, 11 (1972), pp. 599–621.

[11] ———, *Stabilité linéaire des écoulements. Partie II. La couche limite de Blasius*, Journal de Mécanique, 12 (1973), pp. 75–95.

[12] P. Colinet, J.C. Legros, and M.G. Velarde, *Nonlinear dynamics of surface-tension-driven instabilities*, Wiley-VCH, 2001.

[13] I. G. Currie, *The effect of heating rate on the stability of stationary fluids*, Journal of Fluid Mechanics, 29 (1967), p. 337–347.

[14] S. H. Davis, *Thermocapillary instabilities*, Annual Review of Fluid Mechanics, 19 (1987), pp. 403–435.

[15] F. Doumenc, T. Boeck, B. Guerrier, and M. Rossi, *Transient Rayleigh–Bénard–Marangoni convection due to evaporation: A linear non-normal stability analysis*, Journal of Fluid Mechanics, 648 (2010), pp. 521–539.

[16] B. D. Edmonstone, R. V. Craster, and O. K. Matar, *Surfactant-induced fingering phenomena beyond the critical micelle concentration*, Journal of Fluid Mechanics, 564 (2006), p. 105.

[17] T. D. Foster, *Stability of a homogeneous fluid cooled uniformly from above*, Physics of Fluids, 8 (1965), p. 1249.

[18] S. Y. Heriot and R. A. L. Jones, *An interfacial instability in a transient wetting layer leads to lateral phase separation in thin spin-cast polymer-blend films*, Nat Mater, 4 (2005), pp. 782–786.

[19] G. M. Homsy, *Global stability of time-dependent flows: impulsively heated or cooled fluid layers*, Journal of Fluid Mechanics, 60 (1973), p. 129–139.

[20] S. D. Howison, J. A. Moriarty, J. R. Ockendon, E. L. Terrill, and S. K. Wilson, *A mathematical model for drying paint layers*, Journal of Engineering Mathematics, 32 (1997), p. 377–394.

[21] B S Jhaveri and G. M. Homsy, *The onset of convection in fluid layers heated rapidly in a time-dependent manner*, Journal of Fluid Mechanics, 114 (1982), p. 251–260.

[22] K. H. Kang and C. K. Choi, *A theoretical analysis of the onset of surface-tension-driven convection in a horizontal liquid layer cooled suddenly from above*, Physics of Fluids, 9 (1997), p. 7.

[23] J. Kevorkian, *Perturbation techniques for oscillatory systems with slowly varying coefficients*, SIAM Review, 29 (1987), p. 391.

[24] J. Kevorkian and J.D. Cole, *Multiple scale and singular perturbation methods*, Applied mathematical sciences, Springer, 1996.

[25] J. R. King, A. Münch, and B. A. Wagner, *Linear stability analysis of a sharp-interface model for dewetting thin films*, Journal of Engineering Mathematics, 63 (2008), pp. 177–195.

[26] W. Lick, *The instability of a fluid layer with time-dependent heating*, Journal of Fluid Mechanics, 21 (1965), p. 565–576.

[27] C. C. Lin, *Some mathematical problems in the theory of the stability of parallel flows*, Journal

of Fluid Mechanics, 10 (1961), pp. 430–438.
[28] H. Machrafi, A. Rednikov, P. Colinet, and P.C. Dauby, *Bénard instabilities in a binary-liquid layer evaporating into an inert gas: Stability of quasi-stationary and time-dependent reference profiles*, The European Physical Journal Special Topics, 192 (2011), pp. 71–81.
[29] H. Machrafi, A. Rednikov, P. Colinet, and P. C. Dauby, *Bénard instabilities in a binary-liquid layer evaporating into an inert gas*, Journal of Colloid and Interface Science, 349 (2010), pp. 331–353.
[30] E.G. Mahler and R. S. Schechter, *The stability of a fluid layer with gas absorption*, Chemical Engineering Science, 25 (1970), pp. 955–968.
[31] A. Münch and B. Wagner, *Impact of slippage on the morphology and stability of a dewetting rim*, Journal of Physics: Condensed Matter, 23 (2011), p. 184101.
[32] Byaporn NaNagara, Robert D. O'Connor, and Frank D. Blum, *Mobility of toluene in polystyrene-toluene solutions: a NMR study*, The Journal of Physical Chemistry, 96 (1992), pp. 6417–6423.
[33] A.A. Nepomnyashchy, I.B. Simanovskii, and J.C. Legros, *Interfacial convection in multi-layer systems*, Springer monographs in mathematics, Springer, 2006.
[34] J. R. A. Pearson, *On convection cells induced by surface tension*, Journal of Fluid Mechanics, 4 (1958), pp. 489–500.
[35] Lord Rayleigh, *On convection currents in a horizontal layer of fluid, when the higher temperature is under side*, Philosophical Magazine, 32 (1916), pp. 529–546.
[36] S. Rosenblat, *Modulation of thermal convection instability*, Physics of Fluids, 14 (1971), p. 1319.
[37] P. J. Schmid and D. S. Henningson, *Stability and transition in shear flows*, Springer, 2001.
[38] L. E. Scriven and C. V. Sternling, *On cellular convection driven by surface-tension gradients: effects of mean surface tension and surface viscosity*, Journal of Fluid Mechanics, 19 (1964), p. 321–340.
[39] S. F. Shen, *Some considerations on the laminar stability of time-dependent basic flows*, Journal of the Aerospace Sciences, 28 (1961), pp. 397–404 & 417.
[40] K. A. Smith, *On convective instability induced by surface-tension gradients*, Journal of Fluid Mechanics, 24 (1966), p. 401–414.
[41] L. B. Smolka and T. P. Witelski, *On the planar extensional motion of an inertially driven liquid sheet*, Physics of Fluids, 21 (2009), p. 042101.
[42] M. Souche and N. Clarke, *Interfacial instability in bilayer films due to solvent evaporation*, The European Physical Journal E, 28 (2009), pp. 47–55.
[43] O. Touazi, E. Chénier, F. Doumenc, and B. Guerrier, *Simulation of transient Rayleigh-Bénard-Marangoni convection induced by evaporation*, International Journal of Heat and Mass Transfer, 53 (2010), pp. 656–664.
[44] G. Toussaint, H. Bodiguel, F. Doumenc, B. Guerrier, and C. Allain, *Experimental characterization of buoyancy- and surface tension-driven convection during the drying of a polymer solution*, International Journal of Heat and Mass Transfer, 51 (2008), pp. 4228–4237.
[45] B. Trouette, E. Chénier, C. Delcarte, and B. Guerrier, *Numerical study of convection induced by evaporation in cylindrical geometry*, The European Physical Journal Special Topics, 192 (2011), pp. 83–93.
[46] J.S. Vrentas and C.M. Vrentas, *Exchange of stabilities for surface tension driven convection*, Chemical Engineering Science, 59 (2004), pp. 4433–4436.
[47] M. R. E. Warner, R. V. Craster, and O. K. Matar, *Unstable van der Waals driven line rupture in marangoni driven thin viscous films*, Physics of Fluids, 14 (2002), p. 1642.

RECENT REPORTS

31/11	The indentation of pressurized elastic shells: From polymeric capsules to yeast cells	Vella Ajdari Vaziri Boudaoud
32/11	Wrinkling of pressurized elastic shells	Vella Ajdari Vaziri Boudaoud
33/11	Data assimilation using bayesian filters and B-spline geological models	Duan Farmer Hoteit Lu Moroz
34/11	Review of nonlinear Kalman, ensemble and particle filtering with application to the reservoir history matching problem	Luo Hoteit Duan Wang
35/11	Modelling a Tethered Mammalian Sperm Cell undergoing Hyperactivation	Curtis Kirkman-Brown Connolly Gaffney
36/11	A simple mathematical model for investigating the effect of cluster roots on plant nutrient uptake	Zygalakis Roose
37/11	Frequency jumps in the planar vibrations of an elastic beam	Neukirch Frelat Goriely Maurini
38/11	Ice-lens formation and con nement-induced supercooling in soils and other colloidal materials	Style Cocks Peppin Wettlaufer
39/11	An asymptotic theory for the re-equilibration of a micellar surfactant solution	Griffiths Bain Breward Chapman Howell Water
40/11	Higher-order numerical methods for stochastic simulation of chemical reaction systems	Székely Burrage Erban Zygalakis
41/11	On the modelling and simulation of a high pressure shift freezing process	Smith Peppin Ángel M. Ramos
42/11	An efficient implementation of an implicit FEM scheme for fractional-in-space reaction-diffusion equations	Burrage Hale Kay

46/11	A two-compartment mechanochemical model of the roles of transforming growth factor β and tissue tension in dermal wound healing	Murphy Hall Maini McCue McElwain
47/11	Effects of demographic noise on the synchronization of a metapopulation in a fluctuating environment	Lai Newby Bressloff
48/11	High order weak methods for stochastic differential equations based on modified equations	Abdulle Cohen Vilmart Zygalakis
49/11	The kinetics of ice-lens growth in porous media	Style Peppin
50/11	Wound healing angiogenesis: the clinical implications of a simple mathematical model	Flegg Byrne Flegg McElwain
51/11	Wound healing angiogenesis: the clinical implications of a simple mathematical model	Du Gunzburger Lehoucq Zhou
52/11	Image Inpainting based on coherence transport with Adapted distance functions	März
53/11	Surface growth kinematics via local curve evolution	Moulton Goriely

Copies of these, and any other OCCAM reports can be obtained from:

Oxford Centre for Collaborative Applied Mathematics
Mathematical Institute
24 - 29 St Giles'
Oxford
OX1 3LB
England
www.maths.ox.ac.uk/occam